Communications in Mathematics and Applications
Vol. 13, No. 2, pp. 449–459, 2022
ISSN 0975-8607 (online); 0976-5905 (print)
Published by RGN Publications
DOI: 10.26713/cma.v13i2.1795

http://www.rgnpublications.com

Research Article

Radiative Magnetohydrodynamic Flow Over a Vertical Cone Filled With Convective Nanofluid

J.L. Rama Prasad[1], I.V. Venkateswara Rao[1], K.S. Balamurugan[2] and G. Dharmaiah*[3]

[1] *Department of Mathematics, PB Siddartha College of Arts and Science, Vijayawada, Andhra Pradesh, India*
[2] *Department of Mathematics, RVR & JC College of Engineering, Guntur, Andhra Pradesh, India*
[3] *Department of Mathematics, Narasaraopeta Engineering College, Narasaraopet, Andhra Pradesh, India*
***Corresponding author:** dharma.g2007@gmail.com

Received: January 15, 2022 **Accepted:** May 8, 2022

Abstract. This article describes the magnetohydrodynamic radiative nano convective flow over a cone. Brownian motion and thermophoresis effects in nanofluid transport R-K method is used to compute the solutions to the governing non-dimensional partial differential conservation equations and free stream boundary conditions. Numerous thermo-physical parameters were presented, There is a detailed explanation of the simulations as well. Magnetic parameter increases, reduce velocity. According to the findings, there are numerous applications for heat exchanger technology, including geothermal energy storage and cooling, solar energy systems, and materials processing.

Keywords. Magnetohydrodynamics, First order chemical reaction, Thermal radiation, Thermophoresis

Mathematics Subject Classification (2020). 34B05, 34B15, 35G20, 76A99

1. Introduction

Traditional fluids including water, ethylene glycol, xylene, and motor oil are mixed with particle size nanometers to create nanofluids. One of the most important properties of nanofluids is that they have a greater thermal conductivity than traditional fluids. When compared to permissioned fluids, Nanofluids high thermal conductivity is now the most intriguing feature.

Choi and Eastman [5] created a novel liquid, called as Nanofluid on modern coolants and refrigeration technologies. Many researchers [3, 4, 12] have been investigating Nanofluid flow and heat transfer across various geometries while taking diverse physical and chemical characteristics into account over the last few decades. Heat and mass transfer on Casson nanofluid through a nonlinear stretching sheet under boundary profiles with slip conditions were addressed by Rasool *et al*. [17]. The Keller-Box method was used by Rafique *et al*. [16], aimed on the nano liquid flowing through a permeable stretched inclined surface. Unsteady and steady MHD was compared by Sreedevi and Reddy [18] in their research article. Pal *et al*. [15] investigated the effect of a heated stretched surface on a thin nanofluid sheet with thermal radiation. Numerical simulation is done using a shooting method and the Runge-Kutta-Fehlberg integration strategy. Williamson's nanofluid flowed through a vertical narrow cylinder utilising bvp4c in their study by Hussain *et al*. [9]. Al-Khaled and Kahn [1] modeled computationally on microorganisms with changing and activation energy and viscosity. Viscosity and Casson fluid parameters increased together with time, causing an oscillating wall shear force. To better understand the effects of different heat sources and different thermal conductivities on MHD nanofluid flows, Tarakaramu *et al*. [19]. Khan *et al*. [11] used the G.F.E.M to examine thermal management.

In areas including magneto optical wave length optical fibres, pharmacological stimulation, and electromagnetic cell imaging, MHD nano liquids have an extraordinary application. The MHD nano liquid combines the best of liquids and magnetism in a single package. Using a magnetic field has an impact on the dissolved particles, which may change the flow simulation for heat transfer. Anwar *et al*. [2] analysed numerically the radiative MHD flow using the Laplace transformation. Researchers [13, 14, 21] looked into non-newtonian fluid several slip situations.

MHD nanofluid triple diffusion flows through a power law stretched surface were investigated by Goyal *et al*. [6] using Galerkin finite element modelling. They discovered that the nanomass, regular mass, and heat transport rates decreased when the magnetic parameter was amplified owing to an increase in Lorentz drag force. In a partly heated right trapezoidal enclosure, Khan *et al*. [10] addressed radiation impacts and heat augmentation of wate-carbon nanotubes by utilising the Galerkin FEM method. Nanofluid flow across infinitely parallel plates was shown by Usman *et al*. [20], using the modified Legendre wavelets technique in MHD convection. Water-based carbon nanotube heat transfer and hydromagnetic flow were studied by Hamid *et al*. [8] using the Galerkin FEM method in a partly heated rectangular fin-shaped chamber. Chebyshev wavelets were used by Hamid *et al*. [7] to investigate the impact of buoyancy forces on the Williamson nanofluid stagnation point flow.

There have been many literature publications on Nanofluid dynamics in a vertical cone from different angles. Many experimental and hypothetical studies on tube-shaped body transport wonders have been depicted in literature that deals with polymer frameworks' procedure. Heat transfer flow properties of commonly used base fluids such as water, oil, and so on are the primary focus of all of these investigations. Nanofluid research has recently become a popular topic of study because the thermal conductivity of fluids improves when nanoparticles are

present. MHD convection fluxes of Nanofluid through a permeable cone are being investigated in the current research. In both science and engineering, the MHD nanofluid flow analysis is critical. The conservation dimensionless equations are made dimensionless by applying the appropriate non-similar transformations to the data.

2. Modeling of the Problem

We look at a laminar magnetohydrodynamic flow of nano liquid through a cone in a steady state in two dimensions that is incompressible. Figure 1 depicts the problem's physical schematic representation.

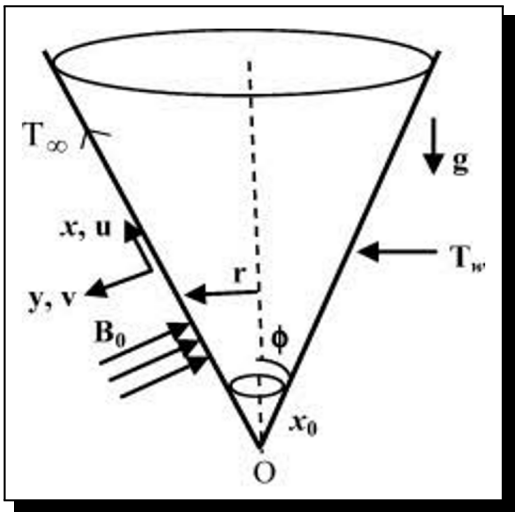

Figure 1. Geometry of the problem

- The cone's surface is subjected to a powerful static magnetic field with a strength of B_0.
- Cone coordinate systems have their origins at their vertex, x-coordinates along the slant surface, and y-coordinates perpendicular to the cone's surface.
- Also, is the cone's radius, and A is the cone's half-angle.
- Gravity's acceleration, measured in units of g, is said to act downwardly.
- Due to the low magnetic Reynolds number, magnetic induction is often ignored.
- Due to the low intensity of the magnetic field, Hall current and ionslip effects are also overlooked.
- Because the flow is so low, Alfven waves are completely ignored.
- Electron and thermo-electric pressures are also neglected in this equation.
- The applied magnetic field B_0 is produced by running a constant current parallel to the cone's longitudinal axis.

The governing equations may be written as follows:

$$\frac{\partial u}{\partial x}+\frac{\partial v}{\partial y}=0, \tag{2.1}$$

$$u\frac{\partial u}{\partial x}+v\frac{\partial u}{\partial y}=\nu\frac{\partial^2 u}{\partial y^2}+g[(1-C_\infty)\rho_f\beta(T-T_\infty)-(\rho_p-\rho_{f\infty})(C-C_\infty)]\cos\phi$$
$$-\frac{\sigma B_0^2}{\rho_f}u-\frac{\mu}{K^*}u, \tag{2.2}$$

$$u\frac{\partial T}{\partial x}+v\frac{\partial T}{\partial y}=\alpha_m\frac{\partial^2 T}{\partial y^2}+\tau\left[D_B\frac{\partial C}{\partial y}\frac{\partial T}{\partial y}+\left(\frac{D_T}{T_\infty}\right)\left(\frac{\partial T}{\partial y}\right)^2\right]-\frac{1}{\rho C_p}\frac{\partial q_r}{\partial y}, \tag{2.3}$$

$$u\frac{\partial C}{\partial x}+v\frac{\partial C}{\partial y}=D_B\frac{\partial^2 C}{\partial y^2}+\left(\frac{D_T}{T_\infty}\right)\frac{\partial^2 T}{\partial y^2}-K_r(C-C_\infty), \tag{2.4}$$

where $\alpha_m=\frac{k_m}{(\rho c)_f}$, and $\tau=\frac{(\rho c)_p}{(\rho c)_f}$.

The relevant boundary conditions are:

$$u=0,\quad v=0,\quad -k\frac{\partial T}{\partial y}=h_f(T_f-T),\quad C=C_w\quad \text{at}\ \ y=0, \tag{2.5}$$

$$u\to 0,\quad T\to T_\infty,\quad C\to C_\infty\quad \text{at}\ \ y\to\infty \tag{2.6}$$

From eqn. (2.1) the stream function ψ is

$$ru=\frac{\partial\psi}{\partial y}\quad\text{and}\quad rv=-\frac{\partial\psi}{\partial x}. \tag{2.7}$$

Introducing dimensionless quantities:

$$\left.\begin{aligned}
&\eta=\frac{y}{x}Ra_x^{\frac{1}{4}}, && f(\eta)=\frac{\psi}{\alpha\, Ra_x^{\frac{1}{4}}},\\
&\theta(\eta)=\frac{T-T_\infty}{T_f-T_\infty}, && \phi(\eta)=\frac{C-C_\infty}{C_w-C_\infty},\\
&Ra_x=\frac{g\beta\rho_{f\infty}(T_w-T_\infty)(1-C_\infty)\cos\gamma x^3}{\mu\alpha}, && Nr=\frac{(\rho_p-\rho_{f\infty})(C_w-C_\infty)}{\rho_{f\infty}\beta(T_w-T_\infty)(1-C_\infty)},\\
&Nb=\frac{\tau D_B(C_w-C_\infty)}{\alpha}, && Nt=\frac{\tau D_T(T_w-T_\infty)}{\alpha T_\infty},\\
&K=\frac{x^2}{k^*\,Ra_x^{\frac{1}{2}}}, && Le=\frac{\nu}{D_B},\\
&Cr=\frac{K_r}{a}, && Pr=\frac{\nu}{\alpha},\\
&R=\frac{16T_\infty^3\sigma^*}{3K^*k}, && M=\frac{\sigma\beta_o^2 x}{\rho Ra_x^{\frac{1}{2}}},\\
&B1=\frac{h_f x}{kRa_x^{\frac{1}{2}}}.
\end{aligned}\right\} \tag{2.8}$$

The obtaining set of non-linear ODEs:

$$f'''-(f')^2+ff''+(\theta-Nr\,\phi)-(M+K)f'=0, \tag{2.9}$$

$$(1+R)\theta''+Prf\theta'+Nb\theta'\phi'+Nt(\theta')^2=0, \tag{2.10}$$

$$\phi''+Le\,f\phi'-Le\cdot Cr\cdot\phi+\frac{Nt}{Nb}\theta''=0. \tag{2.11}$$

The transformed boundary situations are

$$\eta = 0, \quad f = 0, \quad f' = 1, \quad \theta'(0) = -B1(1-\theta(0)), \quad \phi = 1, \tag{2.12}$$

$$\eta \to \infty, \quad f' = 0, \quad \theta = 0, \quad \phi = 0. \tag{2.13}$$

The C_f, Nu_x and Sh_x are:

$$C_f = \frac{2\tau_w}{\rho}, \qquad Nu_x = \frac{xq_w}{k(T_w - T_\infty)}, \quad Sh_x = \frac{xJ_w}{D_B(C_w - C_\infty)}, \tag{2.14}$$

$$\tau_w = \mu\left(\frac{\partial u}{\partial y}\right)_{y=0}, \quad q_w = -k\left(\frac{\partial T}{\partial y}\right)_{y=0}, \quad J_w = -D_B\left(\frac{\partial C}{\partial y}\right)_{y=0}. \tag{2.15}$$

The dimensionless skin friction coefficient, wall temperature and diffusion rates are demarcated as

$$C_f = 2Ra_x^{\frac{3}{4}} f''(0), \quad Nu_x = -Ra_x^{\frac{1}{4}}\theta'(0), \quad Sh_x = -Ra_x^{\frac{1}{4}}\phi'(0). \tag{2.16}$$

3. Numerical Method of Solution

The transformed governing ordinary differential equations (2.12)-(2.14) are highly non-linear. The solution of these equations is more complex due to nonlinearity while solution will get to reduce the complexity. With the 4th order R-K technique we obtained the outcomes.

4. Results and Discussion

Complete calculations are conducted for diverse values of the non-dimensional parameters and the outcomes are illustrated graphically. We considered the following parameter values for entire graphs: $M = 5$; $B_1 = Ra = 0.1$; $Le = 1$; $Pr = 7$; $R = 0.5$; $Cr = 1$; $K = 0.5$, $Nb = Nt = Nr = 0.5$.

Figure 2 shows the impact of the magnetic field parameter on boundary layer velocity drawings. Clearly, when M increases, the hydrodynamic boundary layer thickness decreases (as shown in the image) as indicated. As can be seen in Figure 3, the distribution of velocities differs depending on the chemical reaction parameter. This graph show that when Cr increased, the velocity distribution slowed. To illustrate the influence of Biot number on temperature boundary layer, see Figure 4. As the value of B_1 increases, it seems that the temperature distribution is becoming hotter. On the other hand, Brownian motion and temperature scatterings are shown in Figure 5. The temperature distribution seems to be increased from this figure with increasing values of Nb. Boundary layer temperature drawings in Figure 6 show the strength of buoyancy ratio parameter. As can be seen from this figure, the fluid's heat sketch temperature decreases as the value of Nr increases. Figure 7 shows the temperature scatterings for a wide range of Prandtl numbers. As seen from the figure, the temperature scatterings become slower as Pr gets higher. Figure 8 shows the impact of the thermal radiation parameter on temperature diagrams. Thus, in the boundary layer region, the temperature distribution was enhanced by increasing R intensities. Figure 9 shows the impact of the Lewis number solutal boundary layer. Concentration scatterings seem to improve as Lewis value increases. On the concentration drawings in the boundary layer region, Figure 10 shows buoyancy ratio parameter. As the value of Nr increases, the concentration distributions improve across the fluid region.

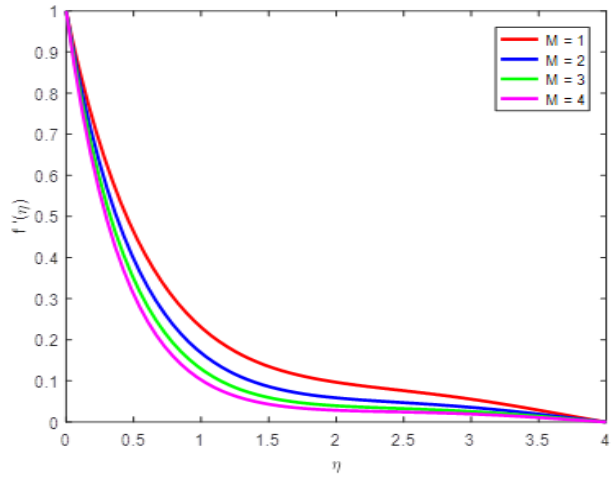

Figure 2. Influence of M on Velocity

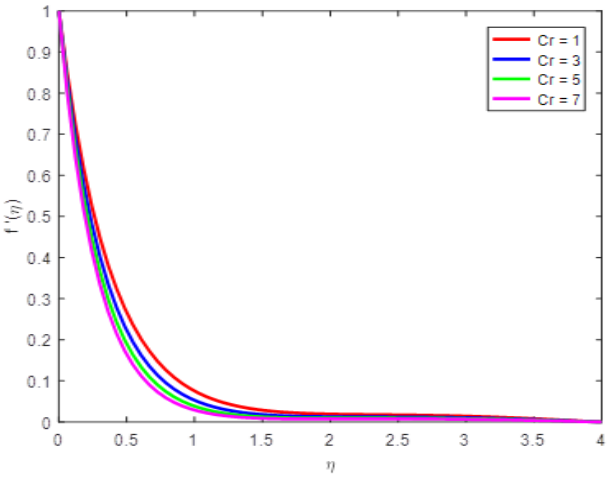

Figure 3. Influence of Cr on Velocity

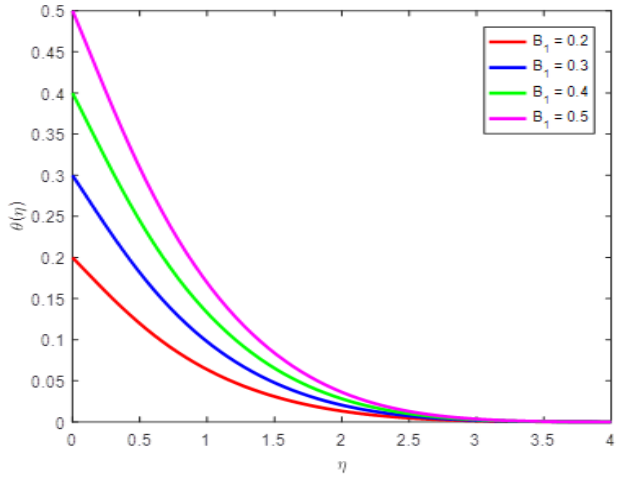

Figure 4. Influence of B_1 on Temperature

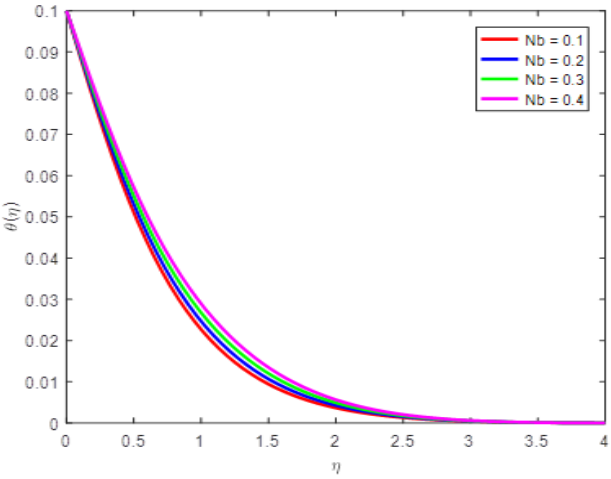

Figure 5. Influence of Nb on Temperature

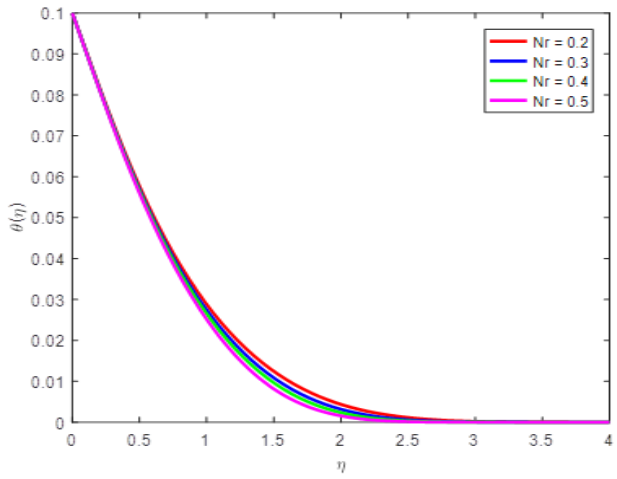

Figure 6. Influence of Nr on Temperature

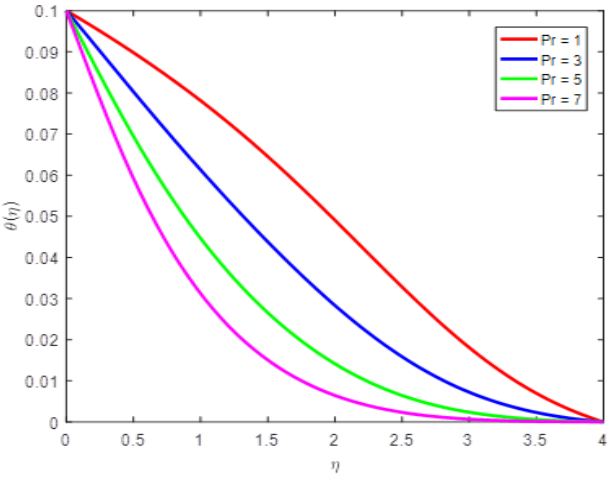

Figure 7. Influence of Pr on Temperature

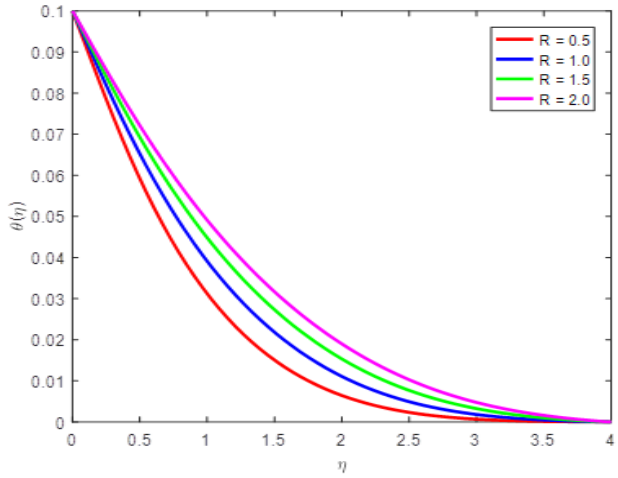

Figure 8. Influence of R on Temperature

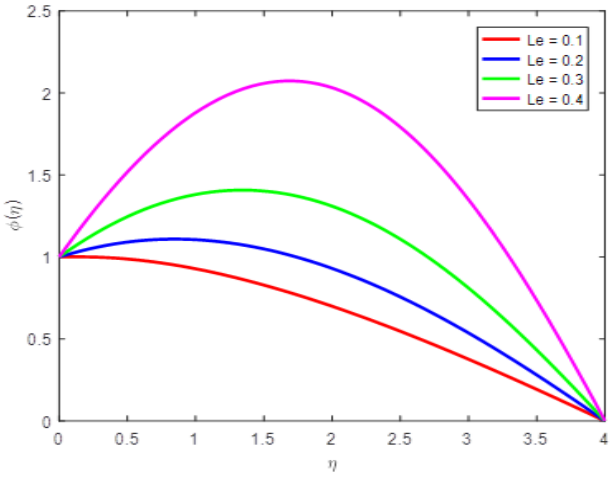

Figure 9. Influence of Le on Concentration

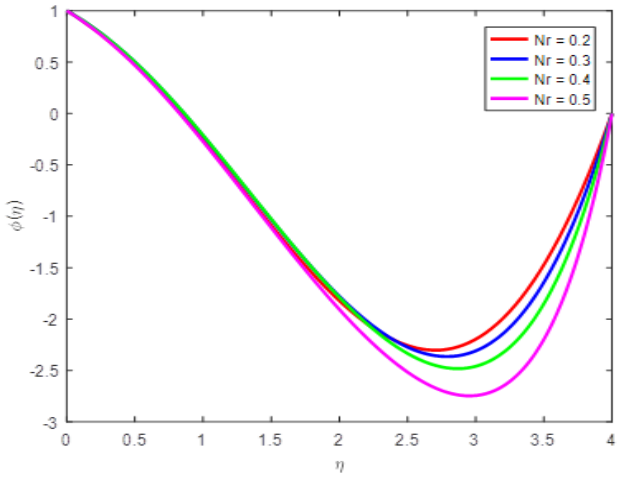

Figure 10. Influence of Nr on Concentration

From Table 1, we have seen Skin-friction increases with increasing of M, Nb, Ra and K while decreases with increasing of B_1, Nt and R. From Table 2, we have seen Nusselt number rises with the amount of B_1 and Ra while falls with the amount of M, Nb, Nt, R and K. From Table 3, we have seen Sherwood increases with increasing of B_1, Nb, Nt and R while decreases with increasing of M, Ra and K.

5. Conclusions

MHD convection fluxes of Nanofluid through a permeable cone are being investigated in the current research. The conservation dimensionless equations are made dimensionless by applying the appropriate non-similar transformations to the data.

Table 1. C_f for various parameter values

M	B_1	Nb	Nt	Ra	R	K	C_f
1	0.1	0.5	0.5	0.1	0.5	0.5	**0.786066**
2	0.1	0.5	0.5	0.1	0.5	0.5	**0.935588**
3	0.1	0.5	0.5	0.1	0.5	0.5	**1.062726**
4	0.1	0.5	0.5	0.1	0.5	0.5	**1.175541**
5	**0.2**	0.5	0.5	0.1	0.5	0.5	**1.276562**
5	**0.3**	0.5	0.5	0.1	0.5	0.5	**1.274983**
5	**0.4**	0.5	0.5	0.1	0.5	0.5	**1.273385**
5	**0.5**	0.5	0.5	0.1	0.5	0.5	**1.271768**
5	0.1	**0.1**	0.5	0.1	0.5	0.5	**1.277820**
5	0.1	**0.2**	0.5	0.1	0.5	0.5	**1.278047**
5	0.1	**0.3**	0.5	0.1	0.5	0.5	**1.278105**
5	0.1	**0.4**	0.5	0.1	0.5	0.5	**1.278122**
5	0.1	0.5	**0.1**	0.1	0.5	0.5	**1.278231**
5	0.1	0.5	**0.2**	0.1	0.5	0.5	**1.278204**
5	0.1	0.5	**0.3**	0.1	0.5	0.5	**1.278176**
5	0.1	0.5	**0.4**	0.1	0.5	0.5	**1.278148**
5	0.1	0.5	0.5	**0.5**	0.5	0.5	**1.292516**
5	0.1	0.5	0.5	**1.0**	0.5	0.5	**1.311968**
5	0.1	0.5	0.5	**1.5**	0.5	0.5	**1.332261**
5	0.1	0.5	0.5	**2.0**	0.5	0.5	**1.352683**
5	0.1	0.5	0.5	0.1	**0.5**	0.5	**1.278120**
5	0.1	0.5	0.5	0.1	**1.0**	0.5	**1.278038**
5	0.1	0.5	0.5	0.1	**1.5**	0.5	**1.277988**
5	0.1	0.5	0.5	0.1	**2.0**	0.5	**1.277956**
5	0.1	0.5	0.5	0.1	0.5	**1**	**1.326637**
5	0.1	0.5	0.5	0.1	0.5	**3**	**1.503703**
5	0.1	0.5	0.5	0.1	0.5	**5**	**1.662018**
5	0.1	0.5	0.5	0.1	0.5	**7**	**1.806412**

Table 2. Nu for various parameter values

M	B_1	Nb	Nt	Ra	R	K	Nu
1	0.1	0.5	0.5	0.1	0.5	0.5	**0.105137**
2	0.1	0.5	0.5	0.1	0.5	0.5	**0.099326**
3	0.1	0.5	0.5	0.1	0.5	0.5	**0.094169**
4	0.1	0.5	0.5	0.1	0.5	0.5	**0.089658**
5	**0.2**	0.5	0.5	0.1	0.5	0.5	**0.167248**
5	**0.3**	0.5	0.5	0.1	0.5	0.5	**0.244827**
5	**0.4**	0.5	0.5	0.1	0.5	0.5	**0.318592**
5	**0.5**	0.5	0.5	0.1	0.5	0.5	**0.388704**
5	0.1	**0.1**	0.5	0.1	0.5	0.5	**0.109666**
5	0.1	**0.2**	0.5	0.1	0.5	0.5	**0.103522**
5	0.1	**0.3**	0.5	0.1	0.5	0.5	**0.097492**
5	0.1	**0.4**	0.5	0.1	0.5	0.5	**0.091548**
5	0.1	0.5	**0.1**	0.1	0.5	0.5	**0.087454**
5	0.1	0.5	**0.2**	0.1	0.5	0.5	**0.087011**
5	0.1	0.5	**0.3**	0.1	0.5	0.5	**0.086570**
5	0.1	0.5	**0.4**	0.1	0.5	0.5	**0.086131**
5	0.1	0.5	0.5	**0.5**	0.5	0.5	**0.087970**
5	0.1	0.5	0.5	**1.0**	0.5	0.5	**0.089954**
5	0.1	0.5	0.5	**1.5**	0.5	0.5	**0.091326**
5	0.1	0.5	0.5	**2.0**	0.5	0.5	**0.092305**
5	0.1	0.5	0.5	0.1	**0.5**	0.5	**0.085695**
5	0.1	0.5	0.5	0.1	**1.0**	0.5	**0.072194**
5	0.1	0.5	0.5	0.1	**1.5**	0.5	**0.063402**
5	0.1	0.5	0.5	0.1	**2.0**	0.5	**0.057245**
5	0.1	0.5	0.5	0.1	0.5	**1**	**0.083890**
5	0.1	0.5	0.5	0.1	0.5	**3**	**0.077630**
5	0.1	0.5	0.5	0.1	0.5	**5**	**0.072571**
5	0.1	0.5	0.5	0.1	0.5	**7**	**0.068394**

Table 3. Sh for various parameter values

M	$B1$	Nb	Nt	Ra	R	K	Sh
1	0.1	0.5	0.5	0.1	0.5	0.5	**1.021001**
2	0.1	0.5	0.5	0.1	0.5	0.5	**0.949505**
3	0.1	0.5	0.5	0.1	0.5	0.5	**0.914947**
4	0.1	0.5	0.5	0.1	0.5	0.5	**0.894974**
5	**0.2**	0.5	0.5	0.1	0.5	0.5	**0.902899**
5	**0.3**	0.5	0.5	0.1	0.5	0.5	**0.926651**
5	**0.4**	0.5	0.5	0.1	0.5	0.5	**0.953293**
5	**0.5**	0.5	0.5	0.1	0.5	0.5	**0.982672**
5	0.1	**0.1**	0.5	0.1	0.5	0.5	**0.868089**
5	0.1	**0.2**	0.5	0.1	0.5	0.5	**0.875201**
5	0.1	**0.3**	0.5	0.1	0.5	0.5	**0.889498**
5	0.1	**0.4**	0.5	0.1	0.5	0.5	**0.891341**
5	0.1	0.5	**0.1**	0.1	0.5	0.5	**0.868157**
5	0.1	0.5	**0.2**	0.1	0.5	0.5	**0.871467**
5	0.1	0.5	**0.3**	0.1	0.5	0.5	**0.874911**
5	0.1	0.5	**0.4**	0.1	0.5	0.5	**0.878486**
5	0.1	0.5	0.5	**0.5**	0.5	0.5	**0.838956**
5	0.1	0.5	0.5	**1.0**	0.5	0.5	**0.800054**
5	0.1	0.5	0.5	**1.5**	0.5	0.5	**0.774713**
5	0.1	0.5	0.5	**2.0**	0.5	0.5	**0.761416**
5	0.1	0.5	0.5	0.1	**0.5**	0.5	**0.882192**
5	0.1	0.5	0.5	0.1	**1.0**	0.5	**0.886815**
5	0.1	0.5	0.5	0.1	**1.5**	0.5	**0.887822**
5	0.1	0.5	0.5	0.1	**2.0**	0.5	**0.887396**
5	0.1	0.5	0.5	0.1	0.5	**1**	**0.877442**
5	0.1	0.5	0.5	0.1	0.5	**3**	**0.864769**
5	0.1	0.5	0.5	0.1	0.5	**5**	**0.857734**
5	0.1	0.5	0.5	0.1	0.5	**7**	**0.853498**

The following observations were found:

- The hydrodynamic boundary layer thickness diminishes with higher values of M.
- The velocity distributions decelerated with the higher values of Cr.
- The velocity distribution elevate as the values of Ra rises.
- The temperature distribution is elevates as the values of B_1 rises.
- With the increasing values of Nb on the temperature distribution elevated.
- The heat sketches of the fluid declines with rising values of Nr.
- The temperature scatterings is retards with the rising values of Pr.
- The temperature distribution enriched with the intensifying values of R.
- The concentration sketches improve in the boundary layer area.

Competing Interests

The authors declare that they have no competing interests.

Authors' Contributions

All the authors contributed significantly in writing this article. The authors read and approved the final manuscript.

References

[1] K. Al-Khaled and S.U. Khan, Thermal aspects of Casson nanoliquid with gyrotactic microorganisms, temperature-dependent viscosity, and variable thermal conductivity: Bio-technology and thermal applications, *Inventions* **5**(3) (2020), Article number 39, pages 14, DOI: 10.3390/inventions5030039.

[2] T. Anwar, P. Kumam, Asifa, I. Khan and P. Thounthong, An exact analysis of radiative heat transfer and unsteady MHD convective flow of a second grade fluid with ramped wall motion and temperature, *Heat Transfer* **50**(1) (2020), 196 – 219, DOI: 10.1002/htj.21871.

[3] J. Buongiorno, Convective transport of nanofluids, *Journal of Heat Transfer* **128** (2006), 240 – 250, DOI: 10.1115/1.2150834.

[4] A.J. Chamkha and A.M. Aly, MHD free convection flow of a nanofluid past a vertical plate in the presence of heat generation or absorption effects, *Chemical Engineering Communications* **198**(3) (2010), 425 – 441, DOI: 10.1080/00986445.2010.520232.

[5] S.U.S. Choi and J.A. Eastman, Enhancing thermal conductivity of fluids with nanoparticles, Developments and applications of non-Newtonian flows, (Conference: 1995 International mechanical engineering congress and exhibition, San Francisco, CA (United States), 12-17 November 1995), *The American Society of Mechanical Engineers* **231** (1995), 99 – 105, URL: https://www.osti.gov/biblio/196525-enhancing-thermal-conductivity-fluids-nanoparticles.

[6] R. Goyal, Vinita, N. Sharma and R. Bhargava, GFEM analysis of MHD nanofluid flow toward a power-law stretching sheet in the presence of thermodiffusive effect along with regression investigation, *Heat Transfer* **50**(1) (2020), 234 – 256, DOI: 10.1002/htj.21873.

[7] M. Hamid, M. Usman, R.U. Haq, Z.H. Khan and W. Wang, Wavelet analysis of stagnation point flow of non-Newtonian nanofluid, *Applied Mathematics and Mechanics* **40**(8) (2019), 1211 – 1226, DOI: 10.1007/s10483-019-2508-6.

[8] M. Hamid, Z.H. Khan, W.A. Khan and R.U. Haq, Natural convection of water-based carbon nanotubes in partially heated rectangular fin-shaped cavity with inner cylindrical obstacle, *Physics of Fluids* **31** (2019), 103607, DOI: 10.1063/1.5124516.

[9] F. Hussain, A. Hussain and S. Nadeem, Thermophoresis and Brownian model of pseudo-plastic nanofluid flow over a vertical slender cylinder, *Mathematical Problems in Engineering* **2020** (2020), Article ID 8428762, DOI: 10.1155/2020/8428762.

[10] Z.H. Khan, W. A. Khan, R.U. Haq, M. Usman and M. Hamid, Effects of volume fraction on water-based carbon nanotubes flow in a right-angle trapezoidal cavity: FEM based analysis, *International Communications in Heat and Mass Transfer* **116** (2020), 104640, DOI: 10.1016/j.icheatmasstransfer.2020.104640.

[11] Z.H. Khan, W.A. Khan, M. Hamid and H. Liu, Finite element analysis of hybrid nanofluid flow and heat transfer in a split lid-driven square cavity with Y-shaped obstacle, *Physics of Fluids* **32** (2020), 093609, DOI: 10.1063/5.0021638.

[12] A.V. Kuznetsov and D.A. Nield, Natural convective boundary-layer flow of a nanofluid past a vertical plate, *International Journal of Thermal Sciences* **49**(3) (2010), 243 – 247, DOI: 10.1016/j.ijthermalsci.2009.07.015.

[13] S. Nadeem, M.N. Khan and N. Abbas, Transportation of slip effects on nanomaterial micropolar fluid flow over exponentially stretching, *Alexandria Engineering Journal* **59**(5) (2020), 3443 – 3450, DOI: 10.1016/j.aej.2020.05.024.

[14] B. Nayak, R.S. Tripathy and S.R. Mishra, Behavior of slip boundary conditions for the flow of nanofluid in the presence of an inclined magnetic field, *Heat Transfer* **49**(8) (2020), 4968 – 4980, DOI: 10.1002/htj.21862.

[15] D. Pal, D. Chatterjee and K. Vajravelu, Influence of magneto-thermo radiation on heat transfer of a thin nanofluid film with non-uniform heat source/sink, *Propulsion and Power Research* **9**(2) (2020), 169 – 180, DOI: 10.1016/j.jppr.2020.03.003.

[16] K. Rafique, M.I. Anwar, M. Misiran and M.I. Asjad, Energy and mass transport of micropolar nanofluid flow over an inclined surface with Keller-Box simulation, *Heat Transfer* **49**(8) (2020), 4592 – 4611, DOI: 10.1002/htj.21843.

[17] G. Rasool, A.J. Chamkha, T. Muhammad, A. Shafiq and I. Khan, Darcy-Forchheimer relation in Casson type MHD nanofluid flow over non-linear stretching surface, *Propulsion and Power Research* **9**(2) (2020), 159 – 168, DOI: 10.1016/j.jppr.2020.04.003.

[18] P. Sreedevi and P.S. Reddy, Heat and mass transfer analysis of MWCNT-kerosene nanofluid flow over a wedge with thermal radiation, *Heat Transfer* **50**(1) (2020), 10 – 33, DOI: 10.1002/htj.21892.

[19] N. Tarakaramu, P.V.S. Narayana and B. Venkateswarlu, Numerical simulation of variable thermal conductivity on 3D flow of nanofluid over a stretching sheet, *Nonlinear Engineering* **9** (2020), 233 – 243, DOI: 10.1515/nleng-2020-0011.

[20] M. Usman, T. Zubair, M. Hamid and R.U. Haq, Novel modification in wavelets method to analyze unsteady flow of nanofluid between two infinitely parallel plates, *Chinese Journal of Physics* **66** (2020), 222 – 236, DOI: 10.1016/j.cjph.2020.03.031.

[21] H. Vaidya, C. Rajashekhar, B.B. Divya, G. Manjunatha, K.V. Prasad and I.L. Animasaun, Influence of transport properties on the peristaltic MHD Jeffrey fluid flow through a porous asymmetric tapered channel, *Results in Physics* **18** (2020), 103295, DOI: 10.1016/j.rinp.2020.103295.